Journal Name

Dynamic Article Links ►

Cite this: DOI: 10.1039/c0xx00000x

www.rsc.org/xxxxxx

ARTICLE TYPE

Dielectric spectroscopy reveals nanoholes in erythrocyte ghosts

Koji Asami*[a]

Received (in XXX, XXX) Xth XXXXXXXXX 20XX, Accepted Xth XXXXXXXXX 20XX
DOI: 10.1039/b000000x

When blood is diluted with water, erythrocytes swell and then burst to release haemoglobin molecules, viz. hypotonic hemolysis. The remaining membranes, so-called "ghosts", have transient holes, which are resealed under physiological conditions. About 50 years ago it was reported that ghost suspensions showed peculiar dielectric dispersion below 10 kHz, termed α-dispersion, which was not found for intact erythrocyte suspensions. The finding, however, has never been traced because of difficulty in low-frequency measurement due to electrode polarization (EP) effects, and therefore the origin of the α-dispersion has not been understood. In this study, the α-dispersion has been revealed using a new type of measurement cell capable of reducing the EP effects. The properties of the α-dispersion were exactly interpreted by modelling ghosts as a spherical cell with a single hole. The numerical simulation with the cell model provided a linear relation between the characteristic frequency of the α-dispersion and the hole radius, thereby the hole radius being determined straightforwardly.

1. Introduction

It is well known that suspensions of intact erythrocytes in physiological saline show dielectric dispersion around 1 MHz (termed β-dispersion) due to interfacial polarization or the Maxwell-Wagner effect, i.e. charges accumulate at interfaces between materials of different electric properties.[1-4] The β-dispersion has been extensively studied to elucidate the electric properties of the plasma membrane and the cytoplasm and the membrane thickness.[5-10] In 1957, Schwan and Carstensen[11] reported that, when erythrocytes were hemolyzed in hypotonic media, low-frequency (LF) dielectric dispersion appeared below 10 kHz in addition to the β-dispersion. The LF dispersion was so-called "α-dispersion" in analogy with that found for some bacterial suspensions[12-14] and various biological tissues.[1,2,15] The α-dispersion of bacteria has a high dielectric increment of more than 10^5 and a relaxation frequency of about 1 kHz, being reasonably assigned to polarization due to counterions near and within the cell wall containing fixed charges at a high density.[12] The counterion polarization has been well studied for charged colloidal suspensions, and a large number of theoretical work has been reported (refer to a review of Grosse and Delgado[16]). However, it seems difficult to interpret the α-dispersion of lysed erythrocytes (ghosts) in terms of the counterion polarization, because the dielectric increment is much smaller than that of bacteria, and because intact erythrocytes, whose membranes have little difference in structure and composition from those of ghosts, do not show the α-dispersion.

To my knowledge the α-dispersion of ghosts has never been investigated since its finding because of difficulty in LF measurement. The α-dispersion is mostly masked by the electrode polarization (EP) effect due to the impedance of the interface between an electrode and an electrolyte solution. A number of methods have been proposed to eliminate or correct the EP effect.[17-22] Nevertheless, there has been no established method, and it is still difficult to get reliable data on the α-dispersion. The origin of the α-dispersion of ghosts, therefore, has not been clearly understood.[23]

Hypotonic hemolysis forms transient holes in erythrocyte membranes, which reseal in physiological conditions.[24] The holes have been characterized by electron microscopy,[25-27] atomic force microscopy[28] and kinetic analysis of efflux and influx of probe molecules through the holes.[29, 30] Seeman[26] reported that ferritin (6 nm in radius) and colloidal gold (≤ 30 nm in radius) were permeable probably through membrane defects of 20-50 nm wide. Lieber and Steck[29, 30] estimated the size and multiplicity of the holes by analysing the diffusion of probe molecules of different sizes through the holes. They concluded that each ghost has a single hole, which contracts to a size of 0.7-14 nm depending on the electrolyte composition of the medium and the incubation temperature. Sato et al.[28] also reported one reversible osmotic hole, and found that the hole formation is closely related to an association of band 3 (or anion exchange) protein, which is the major transmembrane protein of erythrocytes. They proposed that the holes are bordered by a ring of band 3 molecules. The kinetics of the formation and closure of the holes was interpreted in terms of rearrangement of band 3 molecules.[28,31] The holes are relatively stable at 0-4 ºC, and their resealing is much slower than those found in mechanically stretched lipid membrane vesicles.[32-34] This may indicate the participation of membrane proteins in the hole formation of erythrocytes.

During the last decade computer simulation techniques have been developed to investigate dielectric spectra of biological cells of complex morphology.[35-41] In previous papers,[42,43] dielectric spectra have been simulated, within the framework of interfacial polarization, for a spherical cell with a hole by the finite difference method (FDM), implying that the presence of the hole

is responsible for the α-dispersion of ghosts. To verify the theoretical prediction, we need to reveal the properties of the α-dispersion experimentally.

In this paper, the α-dispersion has been studied using a new type of measurement cell that was designed for LF measurement to reduce the EP effect.[44] The properties of the α-dispersion are compared with those calculated by the finite element method (FEM), which provides a more accurate simulation than FDM.

2. Materials and methods

2.1. Preparation of erythrocyte ghosts

Erythrocyte ghosts were prepared from blood specimens of horse, sheep and rabbit purchased from Kojin Bio Ltd. and Nippon Biotest Lab. by the method described in previous papers.[29,30] The blood specimens were centrifuged at 300 × g for 5 min to remove the plasma and the buffy coat, and the collected erythrocytes were washed with a 5 mM Na-phosphate buffer (NaP) (pH 8.0) containing 150 mM NaCl.

One part of the erythrocyte suspension was diluted with 10-20 parts of the haemolysis medium containing 5 mM NaP (pH 8.0) and 0.01 mM $MgSO_4$. The lysed cells were collected by centrifugation at 8000 × g for 15 min and washed with a 5 mM NaP (pH 7.2) buffer with 0.1 mM EDTA to obtain white ghosts whose cytoplasm was fully replaced with the external medium. All operations in the ghost preparation were performed at 0-4ºC.

Ghosts were fixed with 0.1-1 % glutaraldehyde (GA) in 5 mM NaP (pH 7.2) at 0-4 ºC for 1 h.

2.2. Dielectric spectroscopy

In a previous paper,[44] an hourglass-shaped measurement cell was developed to reduce the EP effect in LF measurement. The measurement cell consists of three compartments between platinised Pt-plate electrodes: a small cylindrical sample cavity for a cell suspension between conical compartments filled with the suspending medium. The sample cavity and the neighbouring compartment are separated by dialysis membranes that are freely permeable to ions but not to cells; the electrodes are electrically connected to the sample cavity through the medium. The configuration enables us to increase the electrode surface area and capacitance independently of the sample cavity geometry, which shifts the EP effect toward low frequencies and extend the available LF range. Since the measurement cell leads some errors at high frequencies above 100 kHz, a conventional cell of a parallel-plate capacitor type was also used for correction of the errors.[44]

Dielectric measurement has been carried out over a frequency range of 10 Hz to 10 MHz using a 4192A impedance analyzer (Agilent Technologies). The measurement cells were connected to the impedance analyzer using a 16092A Spring Clip Fixture (Agilent Technologies). One frequency sweep over 61 points was completed within 2 min. The capacitance and conductance measured at frequency f were converted to the complex relative permittivity ε^* defined as $\varepsilon^*=\varepsilon-j\kappa/\omega\varepsilon_0$, where ε is relative permittivity, κ is conductivity, $\omega=2\pi f$, ε_0 is the permittivity of vacuum and j is the imaginary unit.

2.3. Computer simulation by FEM

In previous studies,[42,43] numerical simulation of dielectric spectra was carried out for a spherical cell model with a hole by the three-dimensional FDM. Here, to improve accuracy of the previous simulation especially for a small hole whose radius becomes the same order of the membrane thickness, I adopted FEM that is more appropriate not only for representing the circular hole and the curved cell surface but also for creating meshes flexibly.

Fig. 1A shows the cell model in a cubic unit. The cell interior and the external medium continue through the hole and have the same complex relative permittivity ε_a^* that is $\varepsilon_a^*=\varepsilon_a-j\kappa_a/\omega\varepsilon_0$ with the relative permittivity ε_a and the conductivity κ_a of the aqueous phase. In the cell model, the "thin-layer" approximation[41] was adopted, i.e. the interface between the cell interior and the external medium has zero thickness but the specific admittance of the plasma membrane. Simulation was made for the parallel and perpendicular orientations of the cell model whose symmetric axis through the hole is, respectively, parallel and perpendicular to the applied electric field. When an ac voltage is applied, the distribution of electric potential ϕ in the cubic domain was numerically calculated by a FEM solver COMSOL-Multiphysics (Comsol). The governing equation is the Laplace equation and the boundary conditions are as follows: (i) At the top and bottom boundaries of the cubic domain, electric potentials are given as ϕ=+1, -1 V, respectively. (ii) The boundary between the external medium and the internal phase has a specific admittance Y_m given by $Y_m=G_m+j\omega C_m$. G_m and C_m are, respectively, the specific capacitance and conductance of the plasma membrane defined as $G_m=\kappa_m/d_m$ and $C_m=\varepsilon_m\varepsilon_0/d_m$ with the conductivity κ_m and relative permittivity ε_m of the membrane and the membrane thickness d_m. At the boundary, the electric current density J is related to the electric potential as $n\cdot J_i=n\cdot J_a=(\phi_i-\phi_a)Y_m$, where n is the unit vector normal to the boundary and subscripts i and a refer to the internal phase and the external medium, respectively. (iii) The sides of the cubic domain are insulated electrically and thus $n\cdot J=0$.

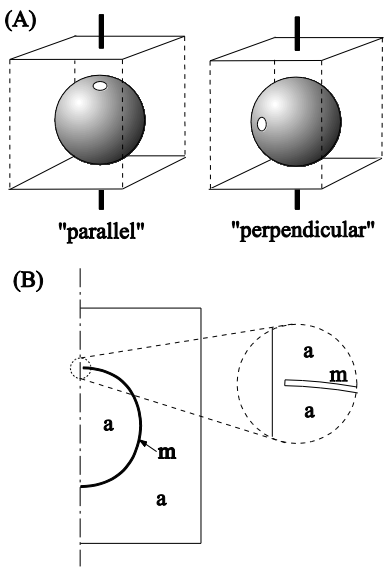

Fig. 1. A spherical cell model with a hole in a cubic unit. (A) 3D models in parallel and perpendicular orientations. An electric field is applied in the direction from the top to the bottom of the cubic unit. (B) A 2D axisymmetry model for the parallel orientation. The dash-dotted line is the symmetric axis. The membrane domain (m) has a uniform thickness, and the aqueous phase (a) continues through the hole

The electric potential distribution provides the current through the cubic domain. Thus, the admittance of the cubic domain was obtained from the current and the applied voltage, being converted to the complex relative permittivity. The complex relative permittivities $\varepsilon_{\perp}^{*}$ and $\varepsilon_{\parallel}^{*}$ calculated, respectively, for the parallel and perpendicular orientations provide the complex relative permittivity ε^{*} of a suspension of the cell models in random orientation as

$$\varepsilon^{*} = \frac{2}{3}\varepsilon_{\perp}^{*} + \frac{1}{3}\varepsilon_{\parallel}^{*}. \quad (1)$$

As the hole radius becomes the same order of the membrane thickness, the thin-layer approximation is not valid and the membrane domain has to be taken into account. However, the thin membrane domain requires extra fine meshes, which generate large computational tasks for the 3D models. Since, for such a small hole, $\varepsilon_{\perp}^{*}$ is the same as the complex relative permittivity of the cell model without a hole,[42,43] calculation can be confined to $\varepsilon_{\parallel}^{*}$, for which a 2D axisymmetric model including the membrane domain (Fig. 1B) is available instead of the 3D model to reduce the computational tasks.

3. Results and discussion

3.1. Dielectric dispersion of ghost suspensions

Ghosts were prepared in a hypotonic medium and were suspended in 5 mM NaP (pH 7.2) containing 0.1 mM EDTA. Immediately after an aliquot of the suspension keeping at 0-4 °C was put into the measurement cell, measurement was carried out at a regular interval at 25 °C. The temperature of the sample suspension quickly reached 25 °C within a few min because of the small sample volume, i.e. about 70 µl. Fig. 2 shows frequency dependence of the relative permittivity ε and conductivity κ measured for the suspension of horse ghosts. The spectrum of the ε at 0 min showed two relaxation processes apart form the EP effect below 1 kHz. The high-frequency (HF) relaxation is the β-dispersion and the LF relaxation corresponds to the α-dispersion reported by Schwan and Carstensen.[11] In succeeding spectra, the LF relaxation moved toward the HF relaxation and the intensities of the LF and HF relaxation both decreased. Finally, the LF relaxation merged into the HF relaxation. Accompanying with the changes of the ε, the κ at low frequencies increased while the HF limit of the κ remained unchanged.

The spectrum change shown in Fig. 2 was retarded by decreasing the measurement temperature and increasing the ionic strength of the medium, and was prevented by fixation of ghosts with glutaraldehyde (GA). GA is known not to influence the electric properties of the plasma membrane.[45, 46] The dielectric spectra of ghosts fixed with 1 % GA at 0-4 ºC for 1 h were quite stable at room temperature. Fixation with 0.1 % GA was not able to stabilize the spectra completely but fairly slowed down the rate of the spectrum change. No discernible effect of the same fixation with 1 % GA was confirmed on dielectric spectra of intact erythrocytes.

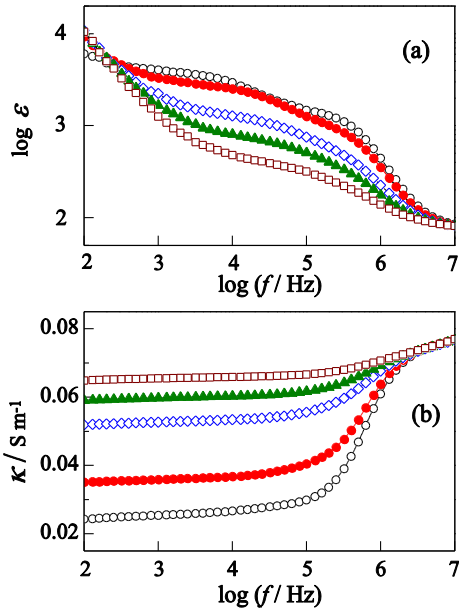

Fig. 2. Frequency dependence of (a) the relative permittivity ε and (b) the conductivity κ of a horse ghost suspension measured at 25 ºC. Data were collected at 0 (○), 5 (●), 11 (◊), 15 (▲) and 25 min (□). Ghosts were suspended in a solution containing 5 mM NaP (7.2) and 0.1 mM EDTA.

Fig. 3a shows the dielectric spectrum for the suspension of ghosts that were fixed with 1 % GA and suspended in a solution containing 5 mM NaP (pH 7.2) and 0.1 mM EDTA. The spectrum was analyzed using an empirical equation including the Cole-Cole relaxation terms[47] and the EP term[17] $A\omega^{-m}$ with constant A and m.

$$\varepsilon^{*} = \varepsilon_{h} + \frac{\Delta\varepsilon_1}{1+(j\omega\tau_1)^{\beta_1}} + \frac{\Delta\varepsilon_2}{1+(j\omega\tau_2)^{\beta_2}} + \frac{\kappa_l}{j\omega\varepsilon_0} + A\omega^{-m}, \quad (2)$$

where ε_h is the HF limit of relative permittivity, $\Delta\varepsilon$ is the relaxation intensity, τ is the relaxation time, β is the Cole-Cole parameter and subscripts 1 and 2 refer to the HF and LF relaxation processes. The characteristic frequencies f_{c1} and f_{c2} are defined as $f_{c1}=(2\pi\tau_1)^{-1}$ and $f_{c2}=(2\pi\tau_2)^{-1}$. The dielectric relaxation parameters were determined by fitting eqn. (2) to the spectrum. The same analysis was made for the spectra of sheep and rabbit ghosts, and the $\Delta\varepsilon_2/\Delta\varepsilon_1$ and the f_{c2}/f_{c1} are summarized in Table 1. The values of $\Delta\varepsilon_2/\Delta\varepsilon_1$ are nearly equal to unity as described by Schwan[1, 23] and are irrespective of animal species, while the values of f_{c2}/f_{c1} are different among animal species.

The spectrum of the ghost suspension was compared with that of intact erythrocytes swollen in a low osmolarity medium containing 5 mM NaP (pH 7.2) and 150 mM mannitol (Fig. 3b). The swollen erythrocytes are of spherical shape similar to that of ghosts, but have intact plasma membranes. The spectrum of the erythrocytes showed only one dielectric relaxation process; LF relaxation was not found down to at least 1 kHz and therefore $\Delta\varepsilon_2=0$ in eqn. (2).

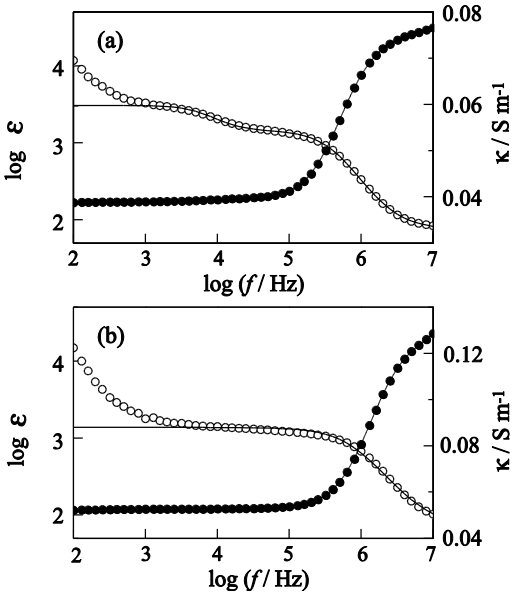

Fig. 3. Dielectric spectra for (a) horse ghosts fixed with 1 % GA and (b) swollen erythrocytes. Open and closed circles are data points of relative permittivity ε and conductivity κ, respectively. The solid lines for ε are the bet-fit curves calculated from eqn. (2), the EP effect being excluded. Temperature is 25 ºC.

The β-dispersion of human and sheep erythrocyte ghosts was analyzed based on the spherical shell-model.[7,48] The estimated values of the membrane capacitance were consistent with those of intact erythrocytes and the conductivity of the inner phase was close to that of the external medium. The same results were obtained in this study.

Table 1. The dielectric relaxation parameters of the suspensions of ghosts from horse, sheep and rabbit erythrocytes

Species	n^a	$\Delta\varepsilon_2/\Delta\varepsilon_1$	f_{c2}/f_{c1}	R/μm[b]	R_h/nm[c]
Horse	8	1.13±0.11	0.0137±0.0023	2.5	152
Sheep	8	1.23±0.04	0.0054±0.0003	2.3	55
Rabbit	9	1.14±0.05	0.0043±0.0005	3.0	57

[a] the number of samples, [b] the cell radii determined by phase contrast microscopy, [c] the hole radii calculated from eqn. (4)

3.2. Effects of medium conductivity and hole size

The responses of the α-dispersion to the change of the medium conductivity κ_a provide a piece of evidence to judge the validity of the theoretical model of ghosts. Hence, the effects of κ_a on the dielectric spectra for ghosts were examined. Ghosts that were fixed with 1 % GA immediately after their preparation were suspended in 0-30 mM NaCl solutions containing 5 mM NaP (pH 7.2) and 0.1 mM EDTA, and were allowed to stand for 1-2 h at 0 ºC to attain equilibrium. Dielectric spectra of the ghost suspensions were measured at 25 °C and their dielectric relaxation parameters were determined. Fig. 4 shows the $\Delta\varepsilon_2/\Delta\varepsilon_1$ and the f_{c2}/f_{c1} plotted for the κ_a. Both of the $\Delta\varepsilon_2/\Delta\varepsilon_1$ and the f_{c2}/f_{c1} were independent of the κ_a within experimental errors.

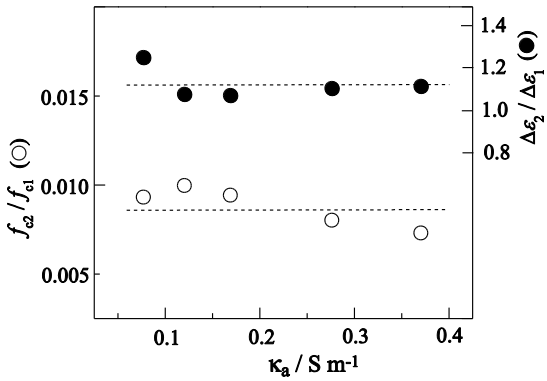

Fig. 4. The f_{c2}/f_{c1} and the $\Delta\varepsilon_2/\Delta\varepsilon_1$ plotted against the medium conductivity κ_a. Ghosts fixed with GA were suspended in buffer solutions containing NaCl at 0-30 mM. The broken lines indicate the average values.

When ghosts are suspended in a medium of elevated ionic strength, their holes are known to decrease in size depending on the incubation temperature and time. To examine the effects of the hole size on the α-dispersion, ghosts of different hole size were prepared under the conditions adopted previously.[30] Ghosts were suspended in a solution containing 15 mM NaCl, 5 mM NaP (pH 7.2) and 0.1 mM EDTA, and were incubated at 0, 15, 25 and 37 ºC. After one-hour incubation the ghosts were fixed with 1 % GA and then suspended in a solution of 5 mM NaP (pH 7.2) and 0.1 mM EDTA to be subjected to measurement. Fig. 5 shows the $\Delta\varepsilon_2/\Delta\varepsilon_1$ and the f_{c2}/f_{c1} plotted for the incubation temperature T. The value of f_{c2}/f_{c1} decreased with increasing T, whereas the value of $\Delta\varepsilon_2/\Delta\varepsilon_1$ remained constant. The results indicate that the decrease in hole radius does not influence the $\Delta\varepsilon_2/\Delta\varepsilon_1$ but decreases the f_{c2}/f_{c1}.

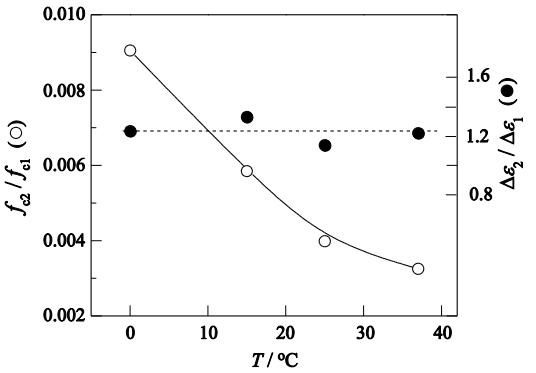

Fig. 5. The $\Delta\varepsilon_2/\Delta\varepsilon_1$ and the f_{c2}/f_{c1} plotted against the incubation temperature T. Ghosts were incubated in a solution containing 5 mM NaP (7.2), 15 mM NaCl and 0.1 mM EDTA at 0, 15, 25 and 37 ºC for 1h and then were fixed with 1 % GA. The fixed ghosts were measured in a solution of 5 mM NaP (pH 7.2) and 0.1 mM EDTA. The broken line for $\Delta\varepsilon_2/\Delta\varepsilon_1$ indicates the average value. The solid curve is drawn as a guide to the eye.

3.3. Numerical simulation with a spherical cell model having a single hole

As a model of ghosts, we consider a spherical cell model of radius R having a single hole of radius R_h (Fig.1). As described in Materials and Methods, effective complex permittivity was calculated for a suspension of cells orienting randomly. In this calculation, polarization due to mobile ions near the membrane having fixed surface charges[49,50] and a resting transmembrane

potential[51] was not taken into account. This is because intact erythrocytes having fixed surface charges like ghosts do not show α-dispersion and because the transmembrane potential becomes zero in ghosts whose cytoplasm is the same as the external medium. The parameter values used for the simulation were ε_a=80, κ_a=0.05 S m^{-1}, ε_m=10, κ_m=0 S m^{-1} and d_m=10 nm.

Fig. 6 shows the relative permittivity plotted for the frequency of the applied ac field. In the case of $R_h \leq$ 200 nm (Fig. 6a), two relaxation processes are clearly seen, both of which have a single relaxation time. The LF relaxation shifts toward low frequencies as decreasing R_h while the HF relaxation is unchanged. The value of $\Delta\varepsilon_2/\Delta\varepsilon_1$ remains unity, and is independent of κ_a. The corresponding conductivity spectra were almost the same because the conductivity increment of the LF relaxation was much less than that of the HF relaxation (data are not shown). When there was no hole, the LF relaxation disappears and the HF relaxation was the same as that calculated from the Pauly-Schwan theory.[52]

For large holes of R_h>0.2 μm (Fig. 6b), the total intensity of dielectric relaxation decreases with increasing R_h and the LF relaxation shifts toward the HF relaxation and merge into one relaxation process. The conductivity at low frequencies increased with R_h (data are not shown).

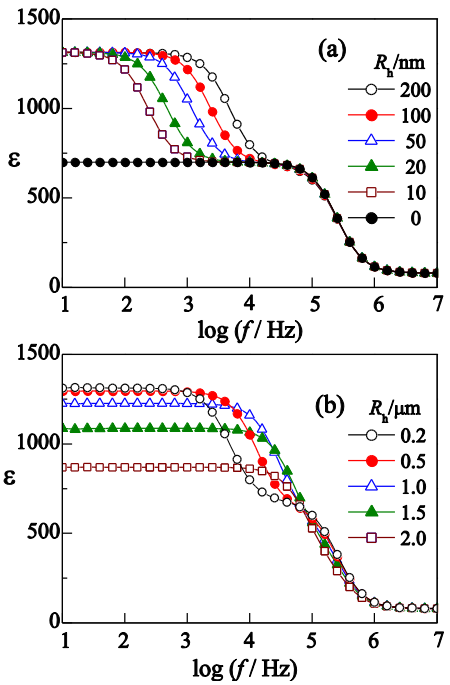

Fig. 6. Frequency f dependence of the relative permittivity ε calculated for the spherical cell model with a hole when the hole radius R_h is (a) smaller and (b) larger than 200 nm. The volume fraction is 0.128. The radius of the spherical cell is 2.5 μm.

Fig. 7 shows double logarithmic plots of the f_{c2}/f_{c1} against the R_h/R. The data points calculated by assuming zero membrane thickness show the linear relationship that is represented by

$$\log(f_{c2}/f_{c1}) = -0.645 + 0.984\log(R_h/R). \quad (3)$$

Eqn. (3) is approximately rewritten by

$$f_{c2}/f_{c1} \approx 0.226(R_h/R). \quad (4)$$

This relationship is independent of the volume fraction of cells and κ_a. When the membrane thickness was taken into account, the data points deviated from Eqn. (3) at R_h/R<0.02. The relationships between f_{c2}/f_{c1} and R_h/R suggest that the hole radius can be estimate from the values of f_{c2}/f_{c1} and R, which are obtainable experimentally.

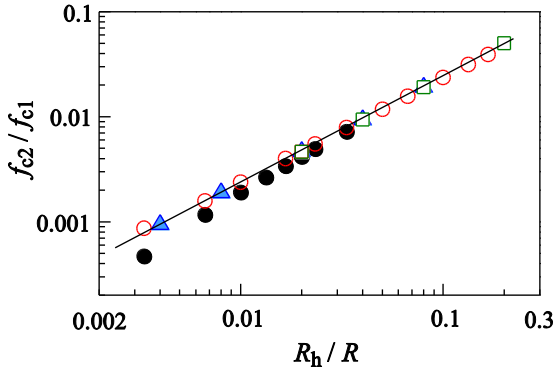

Fig. 7. Double logarithmic plots of the f_{c2}/f_{c1} against the R_h/R. Data points were obtained for R=3 (○), 2.5 (□) and 3.5 μm (▲) by neglecting the effects of the membrane thickness. Data points (●) for R=2.5 include the effects. The solid line is a regression line for the data except points (●).

3.4. Comparison between experimental and theoretical results

The spectrum changes simulated for hole expansion at R_h>0.2 μm (Fig. 6b) are similar to those of ghosts in a low ionic strength medium at 25 ºC (Fig. 2). The holes of ghosts are known to expand in low ionic strength media, e.g. when ghosts were stored in a medium containing 0.5 mM NaP(7.2) and 0.01 mM EDTA at 0 ºC for 8 h, the holes were visible as a single round lesion of 1-3 μm in diameter by dark-field microscopy.[29] Thus, the spectrum changes in Fig. 2 are likely due to the hole expansion.

The experimental results showed that the values of $\Delta\varepsilon_2/\Delta\varepsilon_1$ were close to unity regardless of animal species (Table 1), the value of κ_a (Fig. 4) and reduction in the hole size (Fig. 5). Those are consistent with the numerical simulation, suggesting that each ghost has a single hole. This supports the conclusion of Lieber and Steck[29] and Sato et al.[28] In the previous simulation,[42] when there are two holes in a cell, the value of $\Delta\varepsilon_2/\Delta\varepsilon_1$ decreases from unity with increasing the distance between the two holes. When many small holes evenly distribute on a ghost membrane, the $\Delta\varepsilon_2/\Delta\varepsilon_1$ ratio would be zero.

The values of R_h were calculated from eqn. (4) with the values of f_{c2}/f_{c1} and R obtained experimentally, being summarized in Table 1. Horse ghosts provided a larger value of R_h than sheep and rabbit ghosts. The difference in R_h could result from differences in the lipid and protein compositions of erythrocyte membranes. The distribution of membrane lipids, however, is not large among animal species.[53,54] There is no difference in the content of band 3 protein, which was speculated to participate in formation of osmotic holes, [28] while band 4.2 protein, which is generally accepted as a stabilizing component of erythrocyte membranes, is lacking in horse erythrocyte membranes.[55, 56] The surface charge density of horse erythrocyte membranes is slightly higher than the others,[57, 58] repulsion of the surface charges having a tendency to expand the hole. The absence of band 4.2 protein and the relatively high surface charge density in horse

erythrocyte membranes appear to form larger holes.

The estimated values of R_h are larger than those determined by Lieber and Steck[29, 30] who analyzed the diffusion of probe molecules through the hole of human ghosts, and are rather close to those from electron microscopic studies.[26] It is, however, not easy to exactly compare the values of R_h determined from different methods because experimental conditions were not the same; the hole size depends on temperature, medium compositions and the origin of erythrocytes. Electron microscopy has a risk of artefacts in sample preparation and the measurement of the diffusion of probe molecules requires several procedures and its analysis depends on the model used. I believe that the dielectric method is more straightforward than other methods.

3.5. Relations between membrane disruption and α-dispersion

Osmotic haemolysis disrupts the erythrocyte membrane to make holes, which are the cause of the α-dispersion of ghosts. There have been a few reports implying that the disruption of the plasma membrane causes LF relaxation like the α-dispersion of ghosts. Chelidze found LF relaxation for human blood treated by freezing and thawing and/or by addition of glycerine.[59] The characteristic frequency of the LF relaxation was around 10 kHz and that of the β-dispersion was about 1 MHz. It is known that both of the treatments damage the plasma membrane. Previously, we studied the effects of high hydrostatic pressure on dielectric spectra of human erythrocyte suspensions,[60] and found transient LF relaxation appeared around 10 kHz at 300-400 MPa, where haemolysis occurred. Although there was no clear discussion on the origin of the LF relaxation, the disruption of the membrane could be one of the candidates. It should be noted that Patel et al.[46] discussed the initial increase of the capacitance of yeast suspensions, when treated with 0.5-2 % iso-octanol (v/v), in connection with the membrane disruption.

3.6. Intuitive interpretation of dielectric behaviour of the spherical cell model with a hole

The numerical simulation for the spherical cell model with a hole showed simple dielectric behaviour as: $\Delta\varepsilon_2/\Delta\varepsilon_1$ is unity and f_{c2}/f_{c1} is directly proportional to R_h/R when $R_h/R<0.2$. Here, I try to interpret the dielectric behaviour in terms of equivalent electric circuit models. The LF and HF relaxation processes both have a single relaxation time, which is simply represented by a series combination of a capacitor and a resister.

To derive the expressions of the equivalent capacitance and resistance, we can refer to the electric potential distributions calculated in the numerical simulation. Fig. 8 shows the electric potential distributions that correspond to the spectrum for R_h=50 nm in Fig. 6a. An ac field is applied in the direction from the top to the bottom of the cubic unit by setting +1 V and -1 V to the top and bottom boundaries, respectively. In the frequency region of the HF relaxation (10 kHz-1 MHz), the potential distributions for the parallel and perpendicular orientations both are the same as those from the spherical cell model without hole. The potential inside the cell is 0 V at 10 kHz and 100 kHz, and the cubic unit has an equipotential plane of 0 V at the middle. This means that the upper and lower halves of the spherical cell can be separately dealt with, and that the spherical cell is represented by a serial combination of two capacitors of capacitance $2C_{eq1}$ and a resister of resistance R_{eq1} that correspond to two halves of the cell membrane and the cytoplasm, respectively (Fig. 9b).

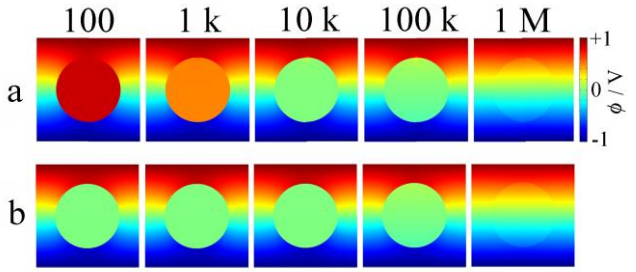

Fig. 8. Electric potential distributions of a spherical cell model with a hole in (a) parallel and (b) perpendicular orientations. The electric potential distributions are shown at a vertical plane through the hole. The frequencies of the applied ac field are shown on the top of the panels.

The HF relaxation is predicted by the Pauly-Schwan theory[52] based on the spherical cell model. When both of the internal phase and the external medium have the same conductivity κ_a that is much larger than the membrane conductivity, an ac field of amplitude E evokes a potential difference at the membrane. The potential difference $\phi_m(\theta)$ at angle θ between the radial vector and the field direction (see Fig. 9a) is given by[2]

$$\phi_m(\theta)=\phi_{mi}(\theta)-\phi_{mo}(\theta)=\frac{1.5ER\cos\theta}{1+j\omega\tau_1}, \tag{5}$$

where ϕ_{mi} and ϕ_{mo} are, respectively, the potentials at the inner and outer surfaces of the cell membrane and

$$\tau_1=\frac{1}{2\pi f_{c1}}=\frac{1.5RC_m}{\kappa_a}. \tag{6}$$

When $\omega\tau_1<<1$, eqn. (5) becomes

$$\phi_m(\theta)=1.5ER\cos\theta. \tag{7}$$

The charge accumulated in the membrane is calculated from the membrane capacitance and the membrane potential difference. We consider an infinitesimally small ring between θ and θ+dθ on the spherical cell. The surface area of the ring is $2\pi R^2\sin\theta d\theta$, and the charge accumulated in the ring becomes $\phi_m(\theta)C_m 2\pi R^2\sin\theta d\theta$. The total charge Q accumulated on the lower half of the cell is calculated by

$$Q=3\pi ER^3C_m\int_0^{\pi/2}\cos\theta\sin\theta d\theta=\frac{3\pi}{2}ER^3C_m. \tag{8}$$

If we assume the effective voltage V applied to the cell as V=2ER, the equivalent capacitance C_{eq1} and resistance R_{eq1} for the HF relaxation become

$$C_{eq1}=\frac{Q}{V}=\frac{3\pi}{4}R^2C_m, \tag{9}$$

$$R_{eq1}=\frac{\tau_1}{C_{eq1}}=\frac{2}{\pi\kappa_a R}. \tag{10}$$

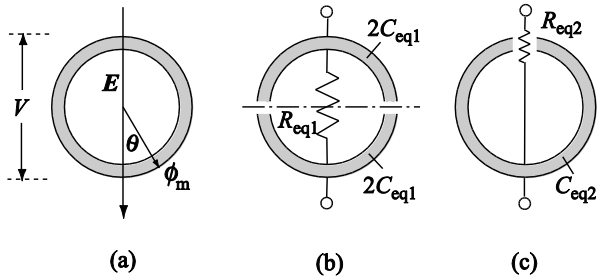

Fig. 9. (a) The membrane potential difference ϕ_m at angle θ evoked by electric field $\boldsymbol{E}$. V is the effective voltage applied to the cell model. (b and c) Equivalent electric circuit models of a spherical cell with a hole in the parallel orientation for (b) HF- and (c) LF-relaxation processes. The dash-dotted line in (b) is an equipotential plane. R_{eq1} and C_{eq1} are, respectively, are the equivalent resistance and capacitance for HF relaxation, and R_{eq2} and C_{eq2} are those for LF relaxation.

Next we will derive the equivalent capacitance C_{eq2} and resistance R_{eq2} for the LF relaxation. Since the perpendicular orientation does not show the LF relaxation,[42, 43] we consider only the parallel orientation. In the LF relaxation region (100 Hz-10 kHz), the potential inside the cell increases with decreasing frequency and has the same potential as that near the hole at the top of the spherical cell at 100 Hz where $\omega\tau_2<<1$. This implies that the LF relaxation is the charging process of the membrane of capacitance C_{eq2} through the hole of resistance R_{eq2} (Fig. 9c).

The membrane potential difference at $\omega\tau_2<<1$ can be obtained as follows. As seen from Fig. 8, it is clear that the potential distributions outside the cell are almost the same independently of the frequency of the applied ac field. Eqn. (7) with $\phi_{mi}=0$ provides $\phi_{mo}=-1.5ER\cos\theta$, and ϕ_{mi} at $\omega\tau_2<<1$ is equal to ϕ_{mo} at $\theta=\pi$, i.e. $\phi_{mi}=1.5ER$, and thus $\phi_m=\phi_{mi}-\phi_{mo}=1.5ER(1+\cos\theta)$. Using the membrane potential difference, the charge accumulated on the whole cell surface is

$$Q=3\pi ER^3C_m\int_0^{\pi}(1+\cos\theta)\sin\theta d\theta=6\pi ER^3C_m. \qquad (11)$$

Using $V=2ER$, C_{eq2} becomes

$$C_{eq2}=3\pi R^2C_m. \qquad (12)$$

The expression of R_{eq2} is provided by a sum of the access resistance and the resistance of the cylindrical hole of radius R_h and length d_m.[61, 62] If the conductivity in the hole is the same as the medium conductivity κ_a, R_{eq2} becomes

$$R_{eq2}=\frac{1}{2R_h\kappa_a}+\frac{d_m}{\pi R_h^2\kappa_a}=\frac{1}{2R_h\kappa_a}\left(1+\frac{2d_m}{\pi R_h}\right). \qquad (13)$$

Eqns. (12) and (13) provide the relaxation time τ_2 for the LF relaxation as

$$\tau_2=\frac{1}{2\pi f_{c2}}\approx R_{eq2}C_{eq2}=\frac{3\pi R^2C_m}{2R_h\kappa_a}\left(1+\frac{2d_m}{\pi R_h}\right). \qquad (14)$$

Finally, the expression of f_{c2}/f_{c1} was obtained from eqns. (6) and (14)

$$\frac{f_{c2}}{f_{c1}}=\frac{\tau_1}{\tau_2}=\frac{1}{\pi}\left(1+\frac{2d_m}{\pi R_h}\right)^{-1}\frac{R_h}{R}. \qquad (15)$$

When $2d_m/(\pi R_h) << 1$, eqn. (15) becomes

$$\frac{f_{c2}}{f_{c1}}=\frac{1}{\pi}\frac{R_h}{R}. \qquad (16)$$

We can get a linear relationship between f_{c2}/f_{c1} and R_h/R as in the numerical simulation, the proportional constant being close to that of eqn. (4) despite the rough derivation. Eqn. (15) explains the deviation from the linear relation when R_h becomes the same order of d_m. Since the equivalent capacitance is proportional to the relaxation intensity, we can obtain

$$\frac{\Delta\varepsilon_2+\Delta\varepsilon_1}{\Delta\varepsilon_1}=\frac{C_{eq2}}{C_{eq1}}=4, \qquad (17)$$

and $\Delta\varepsilon_2/\Delta\varepsilon_1=3$ for the parallel orientation. Since $\Delta\varepsilon_2/\Delta\varepsilon_1=0$ for the perpendicular orientation, using eqn. (1), $\Delta\varepsilon_2/\Delta\varepsilon_1$ for the random orientation becomes unity as obtained by the numerical simulation. .

4. Conclusions

The α-dispersion of erythrocyte ghost suspensions, which was reported by Schwan and Carstensen,[11] has been confirmed using a new type of measurement cell capable of reducing the EP effect. The difficulty of the measurement resulted from not only the EP effect but also instability of the α-dispersion. The α-dispersion diminished quickly at room temperature when ghosts were suspended in low ionic strength solutions, which conditions are known to cause expansion of the holes of ghosts. The α-dispersion was stabilized with GA that is known to fix the hole size of ghosts.[30] The relative intensity of the α-dispersion to the β-dispersion was nearly equal to unity irrespective of the medium conductivity, the volume fraction of ghosts and the size of the holes. The characteristic frequency of the α-dispersion was reduced by decreasing the hole size. The experimental results were consistent with the numerical simulation based on interfacial polarization using the spherical cell model with a single hole. Therefore, the α-dispersion of ghosts can be explained within the framework of interfacial polarization, and is intuitively interpreted in terms of charging of the plasma membrane through the hole.

Acknowledgements

I thank Dr. K. Sekine and Dr. Y. Hayashi for their critical reading of this manuscript and useful comments. This work was supported by Grant-in-Aid for Scientific Research from the Japan Society for the Promotion of Science.

Notes and references

[a] *Institute for Chemical Research, Kyoto University, Uji, Kyoto 611-0011, Japan. Fax: +81 774383084; Tel: +81 774383081; E-mail: asami@e.kuicr.kyoto-u.ac.jp*

1 H. P. Schwan, in *Advances in Biological and Medical Physics*, ed. J. H. Lawrence and C. A. Tobias, Academic Press, New York, 1957, vol. 5, pp. 147-209.
2 K. R. Foster and H. P. Schwan, in *Handbook of Biological Effects of Electromagnetic Fields*, ed. E. C. Polk and E. Postow, CRC Press, Boca Raton, 2nd edn., 1996, ch. 1, pp. 25-102.
3 R. Pethig and D. B. Kell, *Phys. Med. Biol.*, 1987, **32**, 933-970.
4 K. Asami, *Prog. Polym. Sci.*, 2002, **27**, 1617-1659.
5 S. Takashima, K. Asami and Y. Takahashi, *Biophys. J.*, 1988, **54**, 995-1000.
6 K. Asami, Y. Takahashi and S. Takashima, *Biochim. Biophys. Acta*, 1989, **1010**, 49-55.
7 R. Lisin, B. Z. Ginzburg, M. Schlesinger and Y. Feldman, *Biochim. Biophys. Acta*, 1996, **1280**, 34-40.
8 F. Bordi, C. Cametti and T. Gili, *J. Non-Cryst. Solids*, 2002, **305**, 278-284.
9 Y. Hayashi, I. Oshige, Y. Katsumoto, S. Omori, A. Yasuda and K. Asami, *Phys. Med. Biol.*, 2008, **53**, 2553-2564.
10 Y. Hayashi, I. Oshige, Y. Katsumoto, S. Omori, A. Yasuda and K. Asami, *Phys. Med. Biol.*, 2008, **53**, 295-304.
11 H. P. Schwan and E. L. Carstensen, *Science*, 1957, **125**, 985-986.
12 C. E. Einolf and E. L. Carstensen, *Biochim. Biophys. Acta*, 1967, **148**, 506-516.
13 C. E. Einolf and E. L. Carstensen, *Biophys. J.*, 1969, **9**, 634-643.
14 C. E. Einolf and E. L. Carstensen, *Biophys. J.*, 1973, **13**, 8-13.
15 S. Gabriel, R. W. Lau and C. Gabriel, *Phys. Med. Biol.* 1996, **41**, 2251-2269.
16 C. Grosse and A. V. Delgado, *Current Opinion in Collod Interface Sci*. 2010, **15**, 145-159.
17 H. P. Schwan, in *Physical Techniques in Biological Research*, ed. W. L. Nastuk, Academic Press, New York, 1963, vol. 6, ch. 6, pp. 323-406.
18 H. P. Schwan and C. D. Ferris, *Rev. Scie. Instrum.*, 1968, **39**, 481-485.
19 K. Asami, E. Gheorghiu and T. Yonezawa, *Biophys. J.*, 1999, **76**, 3345.
20 V. Raicu, T. Saibara and A. Irimajiri, *Bioelectrochem. Bioenerg.*, 1998, **47**, 325-32.
21 F. Bordi, C. Cametti and T. Gili, *Bioelectrochem.* 2001, **54**, 53-61.
22 Y. Feldman, E. Polygalov, I. Ermolina, Y. Polevaya and B. Tsentsiper, *Meas. Sci. Technol.*, 2001, **12**, 1355-1364.
23 H. P. Schwan, in *The Biophysical Approach to Excitable Systems*, ed. W. S. Adelman and D. Goldman, Plenum Press, New York, 1981, pp 3-24.
24 G. Schwoch and H. Passow, *Mol. Cell. Biochem.*, 1973, **2**, 197-218.
25 D. Danon, *J. Cell. Comp. Physiol.*, 1961, **57**, 111-117.
26 P. Seeman, *J. Cell Biol.*, 1967, **32**, 55-70.
27 P. Seeman, D. Cheng and G. H. Iles, *J. Cell Biol.*, 1973, **56**, 519-527.
28 Y. Sato, H. Yamakose and Y. Suzuki, *Biol. Pharm. Bull.*, 1993, **16**, 506-512.
29 M.R. Lieber and T.L. Steck, *J. Biol. Chem.*, 1982, **257**, 11651-11659.
30 M.R. Lieber and T.L. Steck, *J. Biol. Chem.*, 1982, **257**, 11660-11666.
31 I. Pajic-Lijakovic, V. Ilic, B. Bugarski and M. Plavisc, *Eur. Biophys. J.* 2010, **39**, 789-800.
32 O. Sandre, L. Moreaux and F. Brochard-Wyart, *Proc. Natl. Acad. Sci. USA*, 1999, **96**, 10591-10596.
33 F. Brochard-Wyart, P. G. de Gennes and O. Sandre, *Physica A*, 2000, **278**, 32-51.
34 E. Karatekin, O. Sandre, H. Guitouni, N. Borghi, P.-H. Puech and F. Brochard-Wyart, *Biophys. J.* 2003, **84**, 1734-1749
35 K. Sekine, *Bioelectrochem.*, 2000, **52**, 1-7.
36 M. Sancho, G. Martinez and C. Martin, *J. Electrostat.*, 2003, **57**, 143-156.
37 T. R. Gowrishankar and J.C. Weaver, *Proc. Natl. Acad. Sci. USA*, 2003, **100**, 3203-3208.
38 A. di Biasio and C. Cametti, *Bioelectrochem.*, 2005, **65**, 163-169.
39 K. Asami, *J. Phys. D: Appl. Phys.*, 2006, **39**, 492-499.
40 A. Ron, N. Fishelson, I. Shur, N. Croitoru, D. Benayahu and Y. Schacham-Diamand, *Biophys. Chem.*, 2009, **140**, 39-50.
41 K. Asami, *Jpn. J. Appl. Phys.*, 2010, **49**, 127001.
42 K. Asami, *J. Phys. D: Appl. Phys.*, 2006, **39**, 4656-4663.
43 K. Asami, *Phys. Rev. E*, 2006, **73**, 052903.
44 K. Asami, *Meas. Sci. Technol.*, 2011, **22**,.085801
45 E. L. Carstensen, W. G. Aldridge, S. Z. Child, P. Sullivan and H. H. Brown, *J. Cell Biol.*, 1971, **50**, 529-532.
46 P. M. Patel, A Bhat and G. H. Markx, *Enz. Micrb. Technol.*, 2008, **43**, 523-530.
47 K. S. Cole and R. H. Cole, *J. Chem. Phys.*, 1941, **9**, 341-351.
48 H. Kaneko, K. Asami and T. Hanai, *Colloid Polym. Sci.*, 1991, **269**, 1039-1044.
49 V. Zimmerman and C. Grosse, *J. Phys. Chem.* 2004, **108**, 12617-12622.
50 C. Grosse and V. Zimmerman, *J. Phys. Chem.* 2005, **109**, 18088-18095.
51 E. Prodan, C. Prodan and J. H. Miller, *Biophys. J.* 2008, **95**, 4174-4182.
52 H. Pauly and H.P. Schwan, *Z. Naturforsch.*, 1959, **14b**, 125-131.
53 G. J. Nelson, *Biochim. Biophys. Acta*, 1967, **144**, 221-232.
54 J. A. Virtanen, K. H. Cheng and P. Somerharju, *Proc. Natl. Acad. Sci. USA*, 1998, **95**, 4964-4969.
55 O. K. Baskurt, R. A. Farley and H. J. Meiselman, *Am. J. Physiol. Heart Circ.Physiol.*, 1997, **273**, H2604-H2612.
56 H. Matei, L. Frentescu and G. Benga, *J. Cell. Mol. Med*., 2000, **4**, 270-276.
57 E. H. Eylar, M. A. Madoff, O. V. Brody and J. L. Oncley, *J. Biol. Chem.* 1962, **237**, 1993-2000.
58 G. V. F. Seaman and G. Uhlenbruck, *Arch. Biochem. Biohys.*, 1963, **100**, 493-502.
59 T. Chelidze, *J. Non-Cryst. Solids*, 2002, **305**, 285-294.
60 K. Asami and T. Yamaguchi, *Ann. Biomed. Eng.*, 1999, **27**, 427-435.
61 J. E. Hall, *J. Gen. Phys*., 1975, **66**, 531-532.
62 M. Aguilella-Arzo, V. M. Aguilella and R. S. Eisenberg, *Eur. Biophys. J.*, 2005, **34**, 314-22.